Journal of Alloys and Compounds 936 (2023) 168219

Contents lists available at ScienceDirect

Journal of Alloys and Compounds

journal homepage: www.elsevier.com/locate/jalcom

Computational and experimental investigation of the strain rate sensitivity of small punch testing of the high-entropy alloy CoCrFeMnNi

S. González [a,*], A.K. Sfikas [a], Spyros Kamnis [b], S.E. John [c], Z.W. Nye [c], M. Spink [d], C. Allen [d,g], R. Martínez-Sánchez [e], S.W. Naung [a], M. Rahmati [a], T. Keil [f], K. Durst [f], R.J. Lancaster [c]

[a] Faculty of Engineering and Environment, Northumbria University, Newcastle upon Tyne NE1 8ST, UK
[b] Castolin Eutectic-Monitor Coatings Ltd, Newcastle upon Tyne NE29 8SE, UK
[c] Institute of Structural Materials, Faculty of Science & Engineering, Bay Campus, Swansea University, Swansea SA1 8EN, United Kingdom
[d] Electron Physical Science Imaging Center, Diamond Light Source Ltd, Didcot, Oxfordshire OX11 0DE, UK
[e] Centro de Investigación en Materiales Avanzados [CIMAV], Laboratorio Nacional de Nanotecnología, Miguel de Cervantes 120, 31136 Chihuahua, Chih., Mexico
[f] Materials Science, Physical Metallurgy, Technical University of Darmstadt, Darmstadt D-64287, Germany
[g] Department of Materials, University of Oxford, Oxford OX1 3PH, UK

ARTICLE INFO

Article history:
Received 22 October 2022
Received in revised form 20 November 2022
Accepted 24 November 2022
Available online 29 November 2022

Keywords:
High entropy alloy
Small punch testing
Finite element simulation

ABSTRACT

The suitability of determining the strain rate sensitivity (SRS) of the CoCrFeMnNi high-entropy alloy (HEA) by small punch (SP) testing has been assessed at displacement rates ranging from 0.2 to 2 mm·min^{-1}. The stress was found to increase as the displacement rate was raised from 0.2 to 2 mm·min^{-1}, whereas the plastic strain distributions were similar in all cases. However, for a higher displacement rate of 10 mm·min^{-1}, the sample was found to exhibit a drop in strength and ductility attributed to casting defects. *The strain-rate sensitivity exponent* (m) was found to be 0.1387 whilst the Finite Element Analysis (FEA) simulations predicted a slightly smaller value of 0.1313. This latter value is closer to m = 0.091 obtained from nanoindentation strain rate jump tests since the results are insensitive to the presence of small casting defects. The relationship between the experimental and the empirically derived predicted properties from the SP tests revealed a high level of agreement for maximum stress properties. The properties predicted at 2 mm·min^{-1} (R^2 = 0.96) offered a stronger fit than at 0.5 mm·min^{-1} (R^2 = 0.92).

1. Introduction

High-entropy alloys (HEAs) are a relatively new category of metallic materials that have attracted significant attention over recent years due to the favourable combination of high strength, hardness, corrosion and wear resistance properties that they offer [1–3]. These properties are attributed to the high-entropy, lattice distortion, sluggish diffusion and cocktail effects of the alloys [4]. HEAs are comprised of at least 5 elements with concentrations for each element between 5 and 35 at% [4] and the first references in the literature originated in 2004 when Yeh et al. worked on the concept of HEAs [5] and Cantor et al. worked on multicomponent alloys [6]. Equiatomic CoCrFeMnNi HEAs (otherwise referred to as the Cantor alloys) exhibit many promising properties such as exceptional mechanical behaviour, particularly at lower temperatures [7]. Yet despite the attractive blend of properties that HEAs offer, one of the main limitations of HEAs is their relatively high cost, associated to the expensive materials employed, and the fabrication methods. For this reason, for industrial applications it is of interest to use smaller specimen sizes compared to the geometries commonly employed for mechanical characterization. Moreover, it also provides a more sustainable solution and allows more experimentation when compiling potential compositions. A cost-effective method for testing materials is to use the small punch (SP) test since it offers economic benefits due to the small specimen size, and the potential for more localized assessment of mechanical properties [8]. The use of SP testing has risen in recent decades, where the technique has been employed to mechanically characterise several advanced material systems, such as Ti-6Al-4 V [9,10], and enables additive structures to be tested in three dimensions by extracting material in each of the three principal orientations [8,11]. SP is particularly relevant for testing novel alloys which cannot be produced in large quantities due to prohibitive cost [12]. Among all the mechanical properties that can be obtained from SP testing, including tensile, fracture, creep and fatigue, strain rate sensitivity (SRS) is important since it provides information about the tendency of the tested material to

* Correspondence to: Northumbria University, Newcastle upon Tyne NE1 8ST, UK.
E-mail address: sanchez@northumbria.ac.uk (S. González).

https://doi.org/10.1016/j.jallcom.2022.168219

creep (i.e., no creep when the SRS is zero) and regarding their dynamic mechanical behaviour. These are important properties of multiple engineering components in the aeronautic and energy sectors such as in tubing and piping for power plant boilers, rocket and warhead casings and aircraft landing gears.

Traditionally, the SRS of materials, including HEAs, have been studied under compressive and tensile loads. For example, Park et al. [13] performed quasi-static compression tests on CoCrFeMnNi HEA (Cantor alloy) at strain rates from 10^{-4} s^{-1} (0.024 mm·min^{-1}) to 10^{-2} s^{-1} (2.4 mm·min^{-1}) and obtained a strain-rate sensitivity exponent (m) of 0.028, while for dynamic compression tests at strain rates of ~ 3000, ~3500, and ~4700 s^{-1}, much higher values were obtained, although a number was not given [13]. In fact, the CoCrFeMnNi alloy is the HEA that exhibits highest strain hardening rate compared to other HEAs in dynamic conditions [14], a behaviour similar to that of FCC solid solutions at the conditions of temperature and strain rate studied to date [15]. This behaviour is attributed to the fact that for the quasi-static deformations, rate-controlled dislocation motion is governed by the thermally activated process. However, as the strain rate increases, less time is available to overcome the barrier. This means a lower effectiveness is required to overcome the barrier and therefore the flow stress increases [16]. For this reason, the SRS has an influence on the activation volume of materials (i.e., volume of a material involved in overcoming the energy barrier or rate of decrease of activation enthalpy in regards to the flow stress at a given temperature) [17].

The SRS can be obtained by performing strain rate jump tests (i.e., changing the strain rate during the test). Previously, Shabanisamghabady et al. [16] performed a series of strain rate jump tests on the HEA material CoCrFeMnNi, that exhibited an average grain size of 13 µm. The tests on this material resulted in a strain-rate sensitivity exponent of $m \sim 0.026$ [18]. This value is higher than that of conventional face centred cubic (FCC) metals such as Cu ($m \sim$ 0.006 for 10 nm and $m \sim 0.01$ for 10^4 nm grain size) and Ni ($m \sim$ 0.004 for 10 nm and $m < 0.01$ for 10^4 nm grain size) [19] and similar to that of SP tested stainless steel 316 (i.e., m = 0.018, over a displacement rate range of 0.0125–1.25 mm·min^{-1}) [20]. A decrease in grain size would result in a decrease of the activation volume [21] and the plastic deformation would be governed by a grain boundary -mediated process when the alloy is nanocrystalline [22].

However, to date, there is currently no literature in the public domain that has documented the SRS of the CoCrFeMnNi HEA under small punch testing conditions, despite the previously commented interest in testing smaller specimen sizes.

For the first time, this work presents a study on the feasibility of assessing the SRS of CoCrFeMnNi HEA by using small punch testing. Traditional compression/tension tests to assess the SRS has been mostly performed using chemically homogeneous CoCrFeMnNi HEA after annealing. In this work, however, the CoCrFeMnNi HEA has been fabricated in a single procedure upon casting without subsequent annealing to promote the formation of heterogeneities. This will be of industrial interest as this would lead to a reduction in the number of fabrication steps and will also decrease costs during manufacture. Moreover, the formation of heterogeneities in HEAs has previously been reported to be a useful strategy to promote strength and ductility [23,24].

2. Experimental section

2.1. Materials and microscopy

Alloy ingots with a nominal composition of CoCrFeMnNi (Cantor alloy) were prepared from elements with purity higher than 99.9 at %. The master alloys were remelted (heated to a red heat) multiple times in a Ti-gettered high purity argon atmosphere to attain chemical homogeneity using suction casting arc melting. Cylindrical samples of 8 mm diameter were obtained from the master alloy by copper mold casting in an inert gas atmosphere and a cooling system set at 20 °C. The structure of the as-cast samples was studied by SmartLab Rigaku XRD diffractometer with monochromated Cu Kα radiation (25–90 deg 2θ range). The microstructure was analysed with a scanning electron microscope (SEM) (Mira FEM-SEM Tescan) equipped with energy-dispersive X-ray (EDX) analysis. TEM images were obtained with a JEOL ARM200CF Atomic Resolution Analytical Electron Microscope.

2.2. Mechanical testing

The small punch disc specimens were obtained by sectioning the 8 mm cylinders of the alloy into slices of approximately 800 µm in thickness. Using a custom designed specimen holder, the discs were progressively ground and polished on both faces with finer silicon carbide abrasive papers until the required specimen thickness of 500 µm ± 5 µm with a 1200 grit finish was achieved. These procedures are in direct accordance with the recommendations defined in the EN and ASTM standards for SP testing [25,26]. Small Punch (SP) tensile tests were performed using a bespoke jig, as previously reported in [27]. The jig assembly locates into a 5 kN electric screw test machine and comprises of an upper and lower die set to clamp the SP disc, with a 4 mm diameter receiving hole. The lower die holds a 0.2 mm chamfer above the 4 mm diameter receiving hole, with an initial die entrance of 8 mm diameter to avoid obstruction with the punch geometry. Load is imparted onto the top surface of the disc via a 2.5 mm diameter hemispherical tungsten carbide punch indenter, from which displacement is measured from the test frame cross-head and residual deflection is recorded from the center of the underneath surface of the specimen by a linear variable displacement transducer (LVDT). All tests were performed in accordance with the EN and ASTM standards for SP testing [25,26], under a variety of crosshead displacement rates, ranging from 0.2 to 10 mm·min^{-1}. Each experiment was performed at ambient room temperature in a controlled laboratory environment (21 °C).

Nanoindentation testing was performed at the middle radius of an 8 mm diameter CoCrFeMnNi HEA sample using a G200 nanoindentation system (KLA) equipped with a diamond Berkovich tip (Synton-MDP). The indentation modulus and hardness as well as the strain rate sensitivity of the sample was investigated by strain rate jump tests (SRJ), where the applied strain rate was varied every 500 nm with an indentation depth between 0.05 s^{-1}, 0.005 s^{-1} and 0.001 s^{-1}. The hardness and modulus were measured at an indentation depth interval from 2000 to 2200 nm to minimise the indentation size effect. The SRS was measured using the SRJ from 0.05 s^{-1} to 0.001 s^{-1} at an indentation depth of 1500 nm, which is consistent to the procedures employed in previous publications [28,29].

3. Results and discussion

3.1. Microstructural characterization of as-cast alloy

The microstructure of the 8 mm diameter suction casted CoCrFeMnNi HEA material was studied by X-ray diffraction (XRD), Scanning Electron Microscopy (SEM) and Transmission Electron Microscopy (TEM). The cooling rate, $\dot{T}$, achieved upon casting can be estimated from the relationship [30]:

$$\dot{T}\left(\frac{K}{s}\right) = \frac{10}{R^2}\left(\frac{1}{cm^2}\right) \quad \text{(I)}$$

where R (4 mm) is the sample radius therefore $\dot{T}$ is ~250 K/s. Fig. 1a shows the SEM image corresponding to the middle radius of the sample, the grain size distribution (Fig. 1b) and the corresponding XRD pattern (Fig. 1c). The grain size distribution of has been

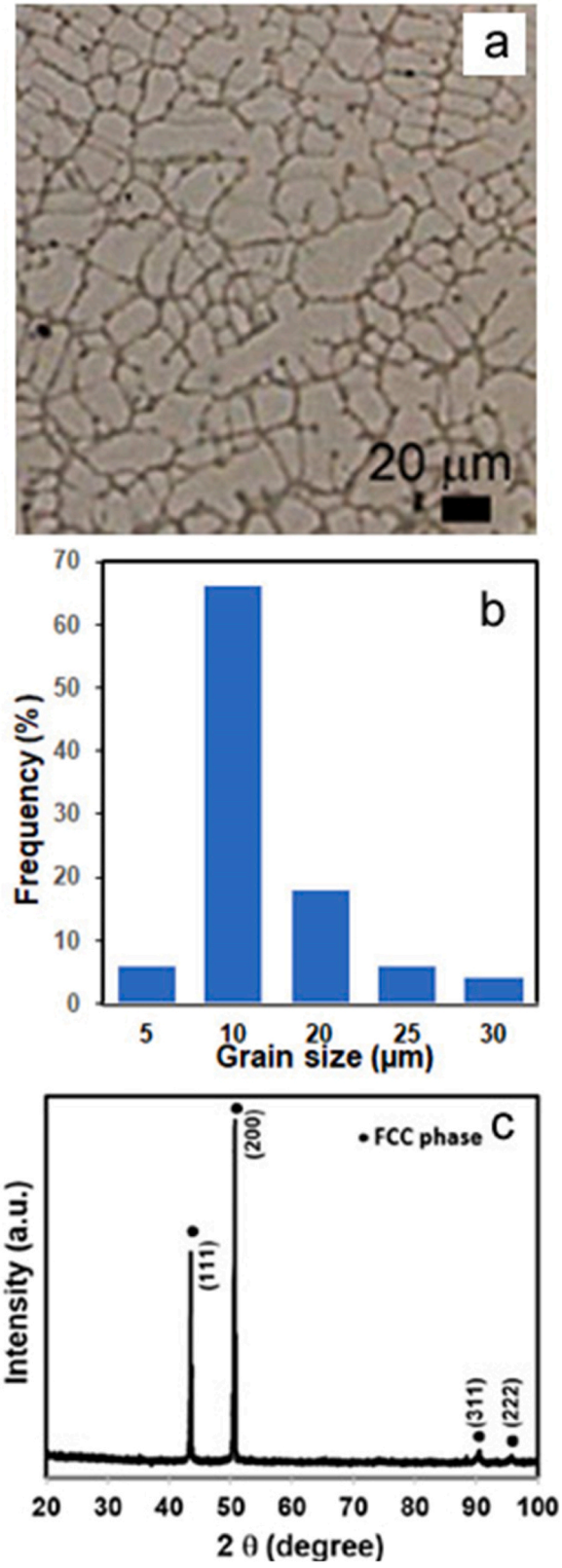

Fig. 1. a) SEM image, b) grain size distribution and c) XRD pattern of the as-cast CoCrFeMnNi HEA suction casted 8 mm diameter cross-section rod.

calculated using the mean linear intercept method [31] and gives an average grain size of 13.2 µm. The XRD scans, presented in Fig. 1c, show that HEA CoCrFeMnNi consists of a single FCC structure with XRD peaks at 43.54°, 50.69°, 90.43° and 95.74°, for which the D-spacings (in Å) of the different (hkl) planes are d(111)= 2.077, d(200) = 1.799, d(311) = 1.085 and d(222) = 1.039 and the lattice constant of CrMnFeCoNi HEA is 3.598 Å, slightly larger than 3.596 Å reported by Li et al. [32] when using Spark Plasma Sintering (SPS) as the fabrication method. The reason for this could be that in suction casting arc-melting, the high cooling rate achieved upon casting promotes a solid solution. However, in SPS annealing takes place and therefore the ability to retain elements in solid solution is lower.

To provide a thorough characterisation of the samples, the composition of the grains have been analysed. The backscattered SEM image and the corresponding compositional X-ray mappings for Mn, Cr, Fe, Co and Ni along with a table listing the chemical composition from Energy-dispersive X-ray (EDX) analysis are shown in Fig. 2. The backscattered SEM image appears featureless with some evenly distributed dark spots. However, the mappings in Fig. 2 show the presence of heterogeneities, a Mn-enriched domain containing Ni and a Cr-Co-Fe- enriched domain with Ni as well. The difference in mechanical properties of these elements will determine the variations in mechanical behaviour of the heterogeneities, as will be discussed later. Nevertheless, the resultant average chemical composition of each element is approximately 20 at%, as listed in Fig. 2. Similar heterogeneities were observed by MacDonald et al. [33] upon casting CoCuFeMnNi HEA. These heterogeneities consisted of dendritic regions rich in Fe and Co and interdendritic regions enriched in Cu and Mn, while the distribution of Ni was constant throughout both regions. For this microstructure, they detected two sets of FCC XRD peaks, a major FCC pattern along a minor FCC pattern shifted to lower angles. However, in the current work with CrMnFeCoNi HEA, the XRD peaks (as given in Fig. 1b) associated to the Mn-enriched and the Co-Cr-Fe-enriched domains completely overlap (i.e., no shifting) thus suggesting both have similar lattice parameters.

3.2. Mechanical properties

In order to understand if the microstructural features detailed in Fig. 2 exhibit consistent mechanical properties, hardness and modulus property maps for the as-cast CoCrFeMnNi HEA have been obtained, as given in Fig. 3a and b, respectively. A representative section from the central radius of the samples of size 70 × 70 µm^2 were tested with the NanoBlitz 3D method. The testing was performed using a grid of 19 × 19 indentations producing a total of 361 indentations, enabling the property maps given in Fig. 3a and b. From the respective colour scales it can be deduced that the average hardness and elastic modulus (E) are approximately 2.75 GPa and 210 GPa, respectively.

The matrix (i.e., the continuous domain) of clear red tonality (Fig. 3) corresponds to the Cr-Co-Fe domain (Fig. 2). However, some darker and lighter domains are also observed. The darker red domains, of approximately 5 µm size, have a hardness of ~3 GPa and a Young's modulus higher than 220 GPa, which could be attributed to the presence of oxides. The light yellow domains may correspond to those areas rich in Mn since it is a soft element with the lowest Young's modulus (E = 198 GPa). In addition, a larger round area with gradient colours from yellow (outside) to dark blue [in the centre) is observed [see bottom of Fig. 3), which could be attributed to the presence of casting defects [i.e., voids). From the representative SEM image of Fig. 2 (volume fraction of dark spots) and Fig. 3 (volume fraction of casting defects), the volume fraction of casting defects have been estimated to be from 0.8 to 1.6 vol%.

3.3. Strain rate sensitivity [SRS)

From the small punch tests, the strain-rate sensitivity [SRS) was calculated to investigate the dependency on the mechanical

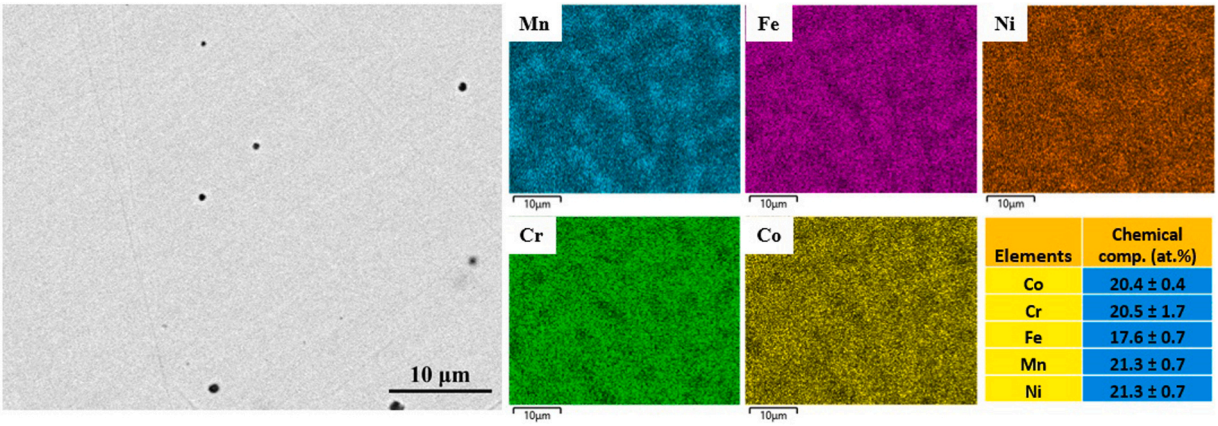

Fig. 2. Backscattered SEM image for CoCrFeMnNi, with corresponding compositional X-ray mappings for Mn, Cr, Fe, Co and Ni and Energy-dispersive X-ray (EDX) results.

performance of the CoCrFeMnNi [Cantor) HEAs. The SRS can be described as [34]:

$$\sigma = K\dot{\varepsilon}^m \tag{II}$$

where the flow stress, σ, is a function of the material constant, K, the strain-rate, and $\dot{\varepsilon}$.

strain-rate sensitivity factor, m. This relationship presumes a linear relationship between the flow stress and the logarithm of strain-rate. From the previous equation, the strain rate sensitivity can be derived as [35]:

$$m = \frac{dln\sigma}{dln\dot{\varepsilon}} \tag{III}$$

where σ and $\dot{\varepsilon}$ represent the flow stress and the strain rate, respectively.

In SP testing, it is generally recognised that four distinct theoretical zones of deformation are observed in a typical force-deflection curve (Fig. 4a) [10]: Zone I corresponds to the elastic region for which the head of the punch has initiated the indentation. Zone II is associated to the progressive extension of plastic bending thus leading to membrane behaviour (i.e., stretching of the membrane around the punch tip) in Zone III. By the end of Zone III, for which the slope of the curve starts to decrease, the membrane stretches to such an extent that the material deforms through necking and cracking, leading to subsequent rupture [Zone IV). From the curve, the effective yield force, F_e, can be obtained by measuring the point at which the tangents of Zone I and Zone II cross (Fig. 4b).

The theoretical curve can be useful when analysing the experimental force-deflection curves (Fig. 5) for the small punch tested CoCrFeMnNi HEA samples under a range of displacement rates (0.2, 0.5, 2 and 10 mm·min^{-1}). The maximum force (F_{MAX}) increases with an increasing displacement rate, from approximately 1300 N at 0.2 mm·min^{-1}, to 1630 N at 0.5 mm·min^{-1}, and to 1700 N at 2 mm·min^{-1}, which is attributed to work-hardening behaviour. However, at 10 mm·min^{-1}, F_{MAX} drops to 1200 N which is thought to be associated to the material embrittling to such a degree that it becomes highly sensitive to the presence of casting defects (see void defects captured in Figs. 2 and 3) caused by work-hardening at such high strain rates that can lead to premature failure. The presence of casting voids may also explain the irregular evolution of the force drop during necking (Zone IV) before F_{MAX} is reached since they promote instability in the materials (i.e., the cross-section reduces faster than the material strain hardening). To minimise the effect of the voids on the results, nanoindentation tests at different strain rates were performed, as will be discussed later in Section 3.5. Given that very small volumes of material are involved in the nanoindentation experiments, this helps to minimise the influence of casting defects on the results. For comparison purposes, the force–deflection behaviour of the CoCrFeMnNi HEA (repeated 4 times as shown in dotted lines to assess repeatability) has been compared to that of commercially available aluminium, copper, Ti-6Al-4 V and stainless steel, under a similar set of testing conditions (0.5 mm·min^{-1}, room temperature). As shown in Fig. 5b, the CoCrFeMnNi HEA exhibits a good combination of strength and ductility, close to that of stainless steel. It also exhibits similar ductility but

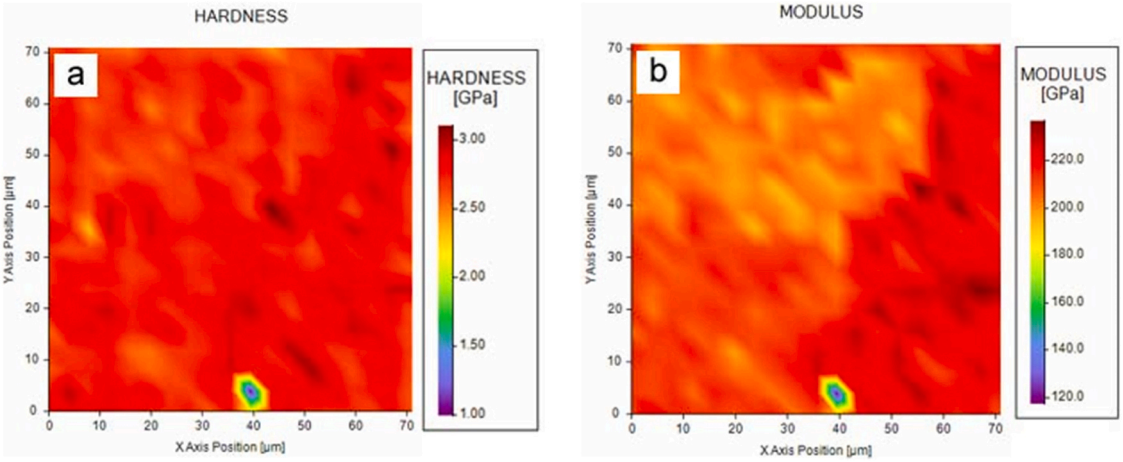

Fig. 3. (a) Hardness and (b) modulus property maps for the as-cast CoCrFeMnNi HEA.

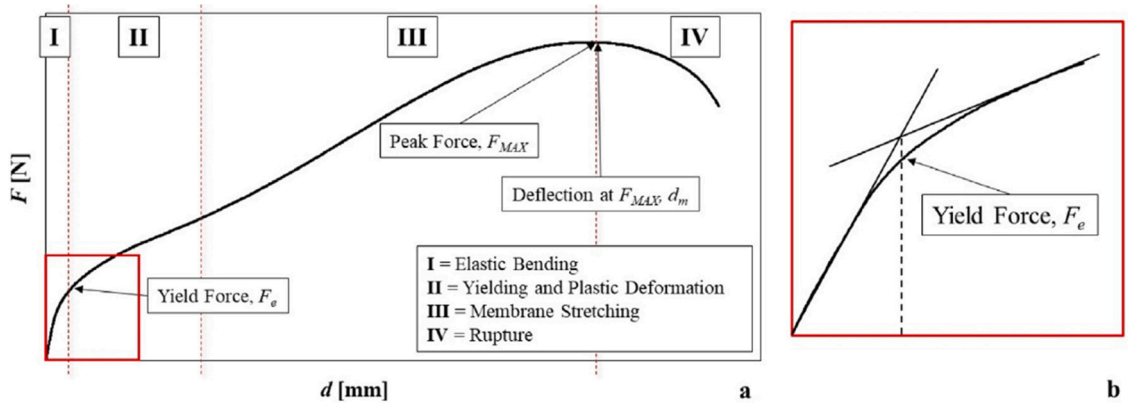

Fig. 4. [a) Example small punch Force-Deflection curve with different deformation zones indicated, [b) Determination of F_e by means of the bilinear method [10].

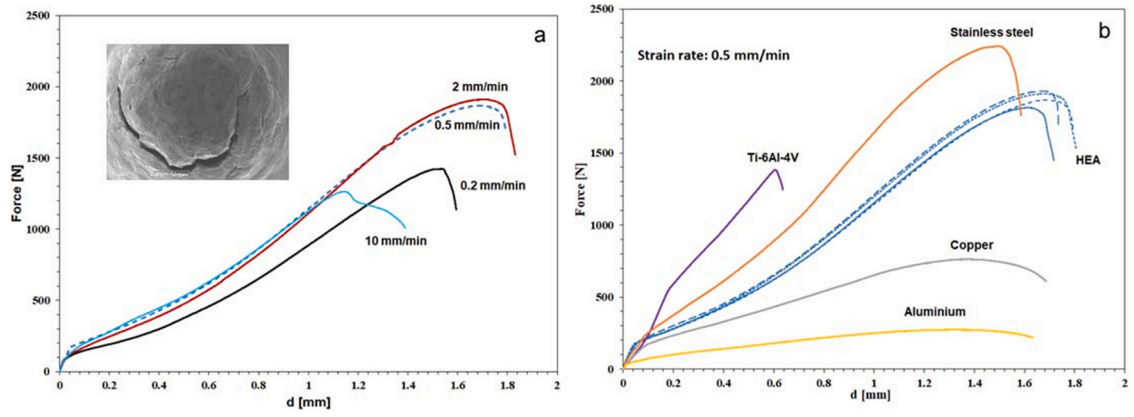

Fig. 5. a) SP force–deflection behaviour of CoCrFeMnN HEA at displacement rates of 0.2, 0.5, 2 and 10 mm·min^{-1} (b) Small punch force–deflection behaviour of four repeat tests on the CoCrFeMnNi HEA and the commercially available aluminium, copper, Ti-6Al-4 V and stainless steel, tested at 0.5 mm·min^{-1}.

higher strength than that of copper and aluminium whilst offering a higher combination of strength and ductility than the titanium alloy, Ti-6Al-4 V.

As discussed, a strain rate increase results in an increase of strength and therefore of the hardness through the following relationship [36]:

$$\sigma_{UTS} / Hv = 3{\cdot}45 \quad \text{(IV)}$$

where Hv is the Vickers hardness and σ_{UTS} is the ultimate tensile strength. These equations were proposed for polycrystalline materials with coarse microstructures and are valid for ideal plastic deformation. Given that in SP testing the stress state is highly biaxial [37], the susceptibility to voids linking (i.e., to failure) tends to increase with biaxial or triaxial stress-states [38]. Therefore in SP the mechanical performance is envisaged to be more sensitive to the presence of defects such as voids originated upon suction casting, than in compression tests. However, in a standard compression test, there are an infinite number of planes available in which failure can take place, upon which the sample will fail along the weakest one available. Furthermore, this would likely be exacerbated by the presence of a defect. Therefore, the SP test could be less sensitive to small cracks, despite the small sample size, but as is the case in compression testing, the proximity of a given defect in the sample also plays a key role. For this reason, it can be concluded that, in the SP test, F_e and F_{MAX} are a function of the displacement rate and therefore it reflects the effect of the strain rate on the mechanical behaviour. However, for brittle materials or materials that embrittle upon work hardening, the results are less reliable. The fact that beyond certain strain rates the strength increase is not as clear, this is consistent with the observations from other authors when SP testing other materials such as commercially pure titanium [37]. For this reason, in order to support the experimental findings, simulations of the SP test results under the different strain rates has been carried out.

3.4. Finite element simulation

3.4.1. Finite element model

Finite element analysis (FEA) simulations using different strain rates were conducted to investigate and visualise the deformation and structural behaviour of the specimen under SP loading. The commercial software ANSYS Mechanical 2021R1 was utilised for the FEA simulations. Fig. 6 shows the numerical model employed in this study. A 2D axisymmetric model was used in this analysis with the specimen being a flexible body whereas the punch indenter, upper die and lower die are all set as rigid bodies for the purpose of computational efficiency.

3.4.2. Loads and boundary conditions

In the simulation, the punch is capable of movement in the vertical direction (Y-direction in Fig. 6), and a constant displacement rate is applied on the punch. In order to validate the FEA model and also investigate the SRS of the structure, the same displacement rates used for the experiments were simulated in the model, namely 0.2, 0.5 and 2 mm·min^{-1}. In each simulation, the specimen was firmly placed between the upper and lower die and the dies were constrained in all directions, whereas frictional coefficients are specified at the contacts between the punch and the specimen, and

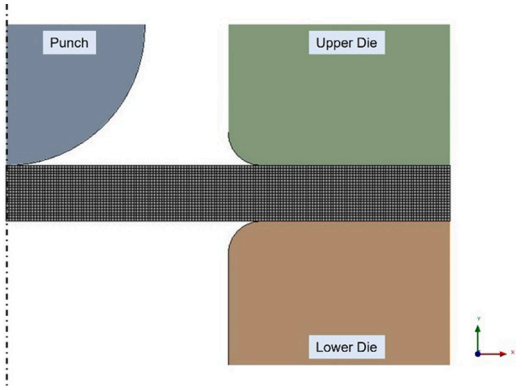

Fig. 6. An axisymmetric numerical model of the small punch test.

between the punch and the dies. The same frictional coefficient of 0.2 is used for all the contacts in this study.

3.4.3. Mesh

An 8-node quadrilateral element type meshing in ANSYS was used to generate the nodes for the specimen, which is treated as a flexible body. A uniform element size of 0.01 mm was used for the entire specimen body, which results in 17 elements in the thickness direction. The generated mesh consisted of 30,490 elements, and the mesh is considered to be sufficient to achieve the required accuracy for the present simulations after conducting the mesh sensitivity analysis. The generated mesh is displayed in Fig. 6.

3.4.4. Numerical setting

In the simulations, large deformation behaviour is activated to account for geometric nonlinearities. The FEA simulation of nonlinear problems are performed using the Newton-Raphson solution method, available in the ANSYS mechanical software. An auto time stepping iteration was selected to ensure the time step was small enough in each iteration and to achieve the solution convergence depending on the amount of load increment.

3.4.5. Material properties

A nonlinear material was created in the Engineering Data module in ANSYS. The linear elastic properties of the material were defined using an isotropic elasticity model. A multi linear isotropic hardening model was also integrated to model the plastic characteristics and nonlinearity of the material subject to loading beyond the elastic limit. To understand the changes in the mechanical properties at the different strain rates, the Johnson–Cook constitutive model [37] was applied to the finite element model. The work hardening behaviour is obtained by fitting Eq. (IV) [39].

In the true stress-true strain curves:

$$\sigma = \sigma_y + k\epsilon^n \tag{V}$$

where σ_y is the yield strength, n is the strain hardening exponent and k is the strength coefficient (strength when strain (ε)= 1). At the reference strain rate, the Johnson–Cook equation can be simplified to:

$$\sigma = A + B\epsilon^n \tag{VI}$$

where A, B and n correspond to the parameters σ_y, k and n respectively. In order to obtain the parameters A, B and n, it is necessary to derive σ_y and ε. However, in SP testing, experimentally these values are difficult to derive, although values of yield force (F_e) and deflection (d) can be determined, from which σ_y and F_e are correlated through an empirical linear relationship as follows [40,41]:

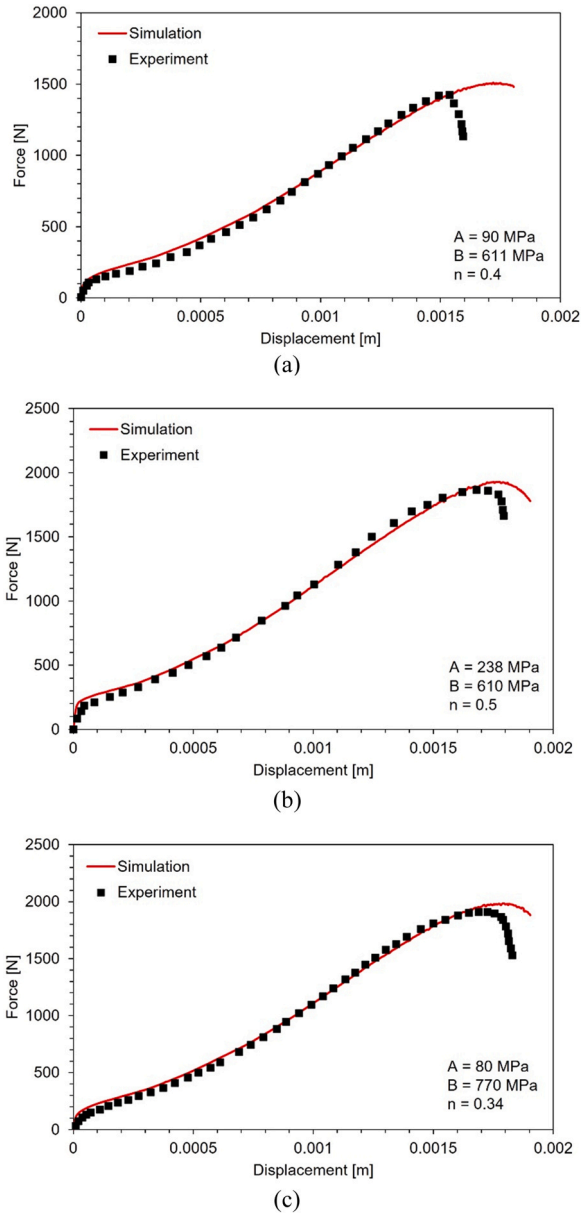

Fig. 7. Finite element simulation results at the different displacement rates of a) 0.2, b) 0.5 and c) 2 mm·min^{-1}.

$$\sigma_{ys} = \alpha_1 \frac{P_y}{t^2} + \alpha_2 \tag{VII}$$

where t is the initial thickness of the disc sample and α_1 and α_2 are test constants. In this case, α_2 is zero, in order for the linear fitting curve to start from the origin. The value of α_1 can be different depending on the material. However, it was previously found that α_1 = 0.346 can provide a good estimation of σ_y for most metallic alloys [41] and it is adopted in this study. The value of F_e is obtained from the vertical projection of the crossing point of the two tangents on the test curve, as previously detailed (see Fig. 4b).

In order to obtain the parameters A, B and n, simulations were performed to replicate the experimental curves from the SP tests obtained at the strain rates of 0.2, 0.5 and 2 mm·min^{-1}. A good agreement between the simulations and experimental results was obtained (see Fig. 7 and Table 1), with a standard error of the estimated R^2 values ranging from 0.92 to 0.96. These results show that the first three regions of the simulation curves at the different strain rates fit well with the experimental curves and therefore enables

Table 1
Parameters *A*, *B*, *n* and error R^2 values extracted after fitting the Johnson–Cook equation.

Strain rate [mm·min^{-1}]	A parameter [MPa]	B parameter [MPa]	n parameter	σ_{max} Experimental [MPa]	σ_{max} Predicted [MPa]	R^2
0.2	90	611	0.40	601.45	615	0.93
0.5	238	610	0.50	815.70	820	0.92
2	80	770	0.34	846.69	850	0.96

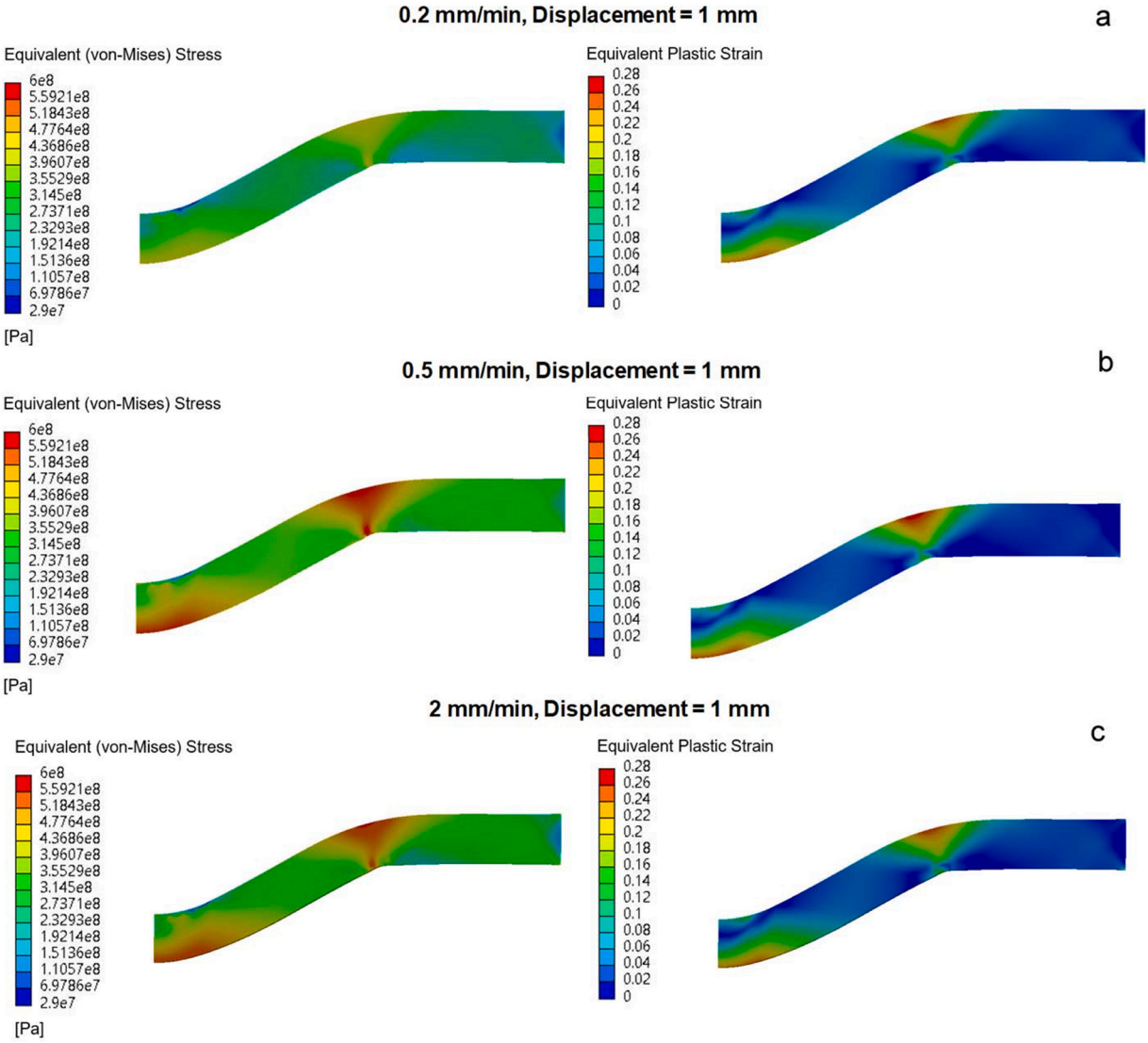

Fig. 8. Von Mises stress and equivalent plastic strain of the specimen for displacement rates of [a) 0.2 mm·min^{-1}, (b) 0.5 mm·min^{-1} and (c) 2 mm·min^{-1} after 1 mm deflection.

accurate parameters to be derived. However, for the plastic region beyond the maximum force, there is a period of plastic instability for which the fitting is not as accurate, which is consistent with previous reports [42]. This necking instability is associated with void coalescence, a phenomena expected from the presence of voids in the as-cast sample (Figs. 2 and 3). Therefore, this enables an accurate value of the strain rate sensitivity without the influence of casting defects to be determined. As commented previously, another method to prevent the presence of casting defects affecting the reliability of the results is from nanoindentation experiments (Section 3.5). One of the benefits of performing an FEA simulation is that the stress distribution due to internal and external forces can be both qualitatively and quantitatively analysed. At the same time, the corresponding stress and strain relationship can also be identified. Fig. 8 shows the simulated von Mises and equivalent plastic strain distribution of the CoCrFeMnNi HEA material under SP loading under different displacement rates, after the simulations have reached a fixed deflection of 1 mm. When the load is exerted onto the indenter under SP loading, internal forces are distributed throughout the structure of the specimen, and consequently, the specimen is deformed as it is compressed by the punch. The shape of the deformation of the specimen is dominated by the punch head diameter. As the specimen is pressed downwards by the head of the indenter, a reaction force occurs at the supports with the dies. Therefore, it is observed that the stress is concentrated in the contact regions where the specimen is in contact with the punch head and the dies. There is local yielding with a maximum stress zone on the lower surface of the specimen as the punch pushes through the specimen, and the area in close proximity to the supports, where both regions undergo the plastic bending stage. The stress distribution in the specimen at a faster displacement rate is generally greater than that of a slower displacement rate. When the

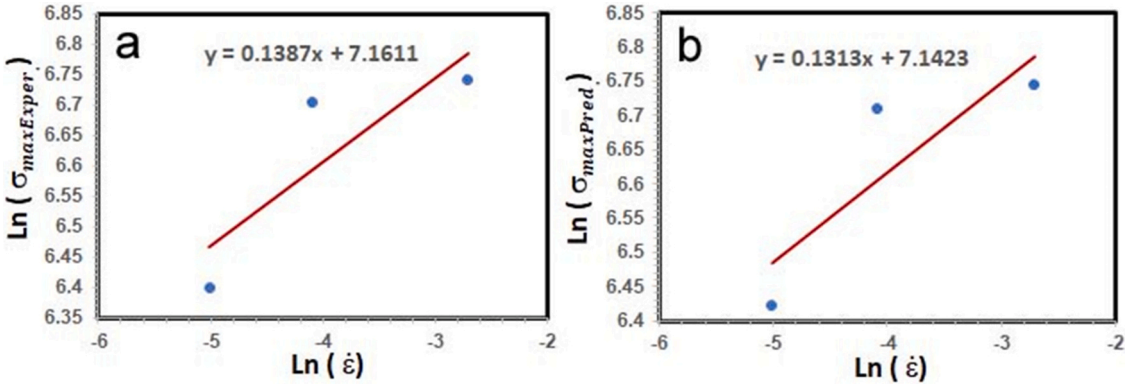

Fig. 9. Plot Ln max. stress-Ln strain rate for the a) experimental and b) predicted stresses.

displacement rate increases from 0.2 to 0.5 mm·min^{-1}, the equivalent von Mises stress in the specimen increases from a maximum of approximately 3.96×10^8 Pa (as indicated by the green colour on the lower surface of the specimen) to more than 5.5×10^8 Pa (as given by the red colour on the lower surface of the specimen). However, when a strain rate of 2 mm·min^{-1} is reached, no significant differences in the equivalent von Mises stress is observed, which is consistent with the force–deflection curves (Fig. 8). The stress is then distributed into a wider area in the radial direction and also through the specimen thickness. At the same time, the plastic strain also starts to build up at these contact regions. The equivalent plastic strain is basically the same, as could be expected considering that the analysis has been performed to the same fixed deflection of 1 mm. This deflection falls within the region of membrane stretching but the stretching is not significant as can be deduced from the fact that there is practically no reduction of thickness of the specimen due to thinning. The shape of the deformation of the specimen and the development of plastic zones are in good agreement with other published findings [42].

In order to calculate the SRS, two separate plots are derived; the Ln of the strain rate versus the Ln of the maximum experimental stress (Fig. 9a) and the Ln of the strain rate against the maximum theoretical predicted stress (Fig. 9b). The plots have been obtained from the values listed in Table 1. From the experimental results, a SRS value of m = 0.1387 is obtained, while for the predicted correlation, a slightly smaller value is derived, m = *0.1313*. These values are similar to those of nanocrystalline titanium (m = 0.163) [43] although the crystalline structure of Ti is hexagonally closed packed (HCP) while for the Cantor alloy, it is FCC. Therefore, it is important to take into consideration that m depends both on the grain size of the material and the applied strain rate and therefore will be the topic of our future investigations.

For high purity Cu, an FCC metal, when the material is tested in tension, Carreker and Hibbard [44] observed that m ranges from 0.004 to 0.0072 for a grain size range of 12–90 µm, while for a smaller grain size of 40 µm, m ~0.006, as reported by Follansbee et al. [45]. However, for very slow strain rates, FCC metals such as Ni, Au and Cu exhibit m values even greater than ~0.5. According to Wei et al. [46] the high m values observed in such materials can be attributed to the fact that at very slow strain rates, deformation would be controlled by diffusional mechanisms such as grain boundary sliding (m = 0.5).

However, as previously commented, the experimental and predicted SRS values are different since in SP testing, the samples are subjected to a biaxial stress state and therefore the samples are subjected to high strain conditions. As such, the mechanical performance is more sensitive to the presence of defects such as those observed in Figs. 2 and 3. To further investigate this, nanoindentation tests were performed to provide a more localized technique of obtaining mechanical properties from very small volumes of materials to limit the influence of internal flows present in the material.

3.5. Nanoindentation strain rate jump testing

A series of nanoindentation tests were performed to generate hardness and indentation modulus properties (Fig. 10). Tests were performed at a constant strain rate of 0.05 s^{-1} at an indentation depth interval from 2000 to 2200 nm. Fig. 10 shows that hardness decreases with increasing indentation depth, which is caused by the indentation size effect (ISE). According to Nix and Gao, this phenomenon is attributed to the variation in the density of the

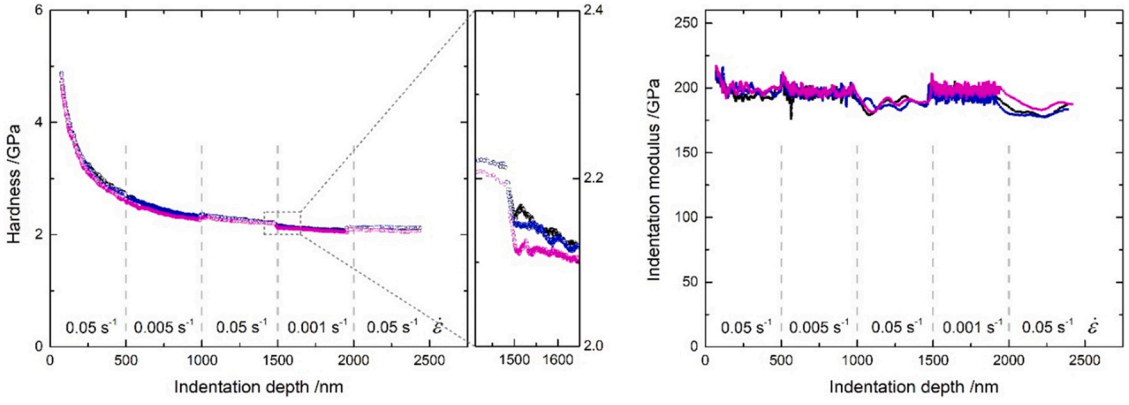

Fig. 10. Hardness and modulus vs. indentation depth of the Cantor alloy from nanoindentation SRJ testing. Only three representative curves are shown to improve the readability of the figure.

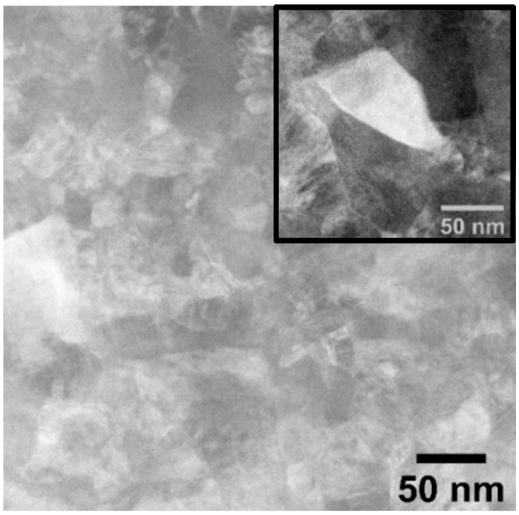

Fig. 11. shows the TEM image for CoCrFeMnNi HEA is the as-cast condition. Inset: magnified TEM image showing ultrafine grains.

generated geometrically necessary dislocations (GNDs) underneath the indenter [47]. For the indentation depth interval of 2000–2200 nm, the hardness and modulus have already reached a depth independent plateau. Therefore, the mechanical properties have been averaged over this depth interval in order to minimise the influence of the ISE. From this indentation depth interval, a hardness of 2.17 ± 0.06 GPa and a Young's modulus of 184 ± 8 GPa are obtained.

According to Gludovatz et al. [48], for the chemically homogeneous CrMnFeCoNi HEA, the hardness is 1.422 GPa (145 HV) and the Young's modulus 202 GPa, which are therefore slightly different from those reported here. The higher hardness (i.e., 2.17 ± 0.06 GPa) is attributed to the high lattice resistance to dislocation movement since they have to navigate through the heterogeneities [23] whilst the relatively low Young's modulus (i.e., 184 ± 8 GPa) could be associated to the presence of a Mn-enriched domain which exhibits a reduced stiffness. The presence of heterogeneities was also reported to enhance the mechanical performance of other compositions such as $Fe_{40}Mn_{20}Cr_{20}Ni_{20}$ HEA under quasi-static and dynamic conditions [49] or in CrFeNi medium-entropy alloy, achieving a good strength-ductility tradeoff [50].

The SRS exponent $m = \frac{d(\ln H)}{d(\ln \dot{\varepsilon})}$ was determined using the SRJ tests at an indentation depth of 1500 nm, from 0.05 s^{-1} to 0.001 s^{-1}, similar to that previously reported [51]. From the SRJ tests, an m value of 0.0091 is obtained. This value is comparable to the results obtained from Maier-Kiener et al. [28] on coarse-grained Cantor who also used nanoindentation STJ testing (m = 0.008). This value is smaller than the values obtained from the SP tests, which were 0.1313 (predicted) and 0.1387 (experimental) (as shown in Fig. 10) but closer to the predicted result, since the small volume of material tested in nanoindentation results in values closer to the theoretical ones for which no casting defects would be present. A useful parameter in nanomechanical testing is the activation volume, V^*, since it represents the number of atoms involved in the deformation [52] and therefore provides information about the mechanism responsible for the plastic deformation behaviour (thermally-activated processes during plastic flow). The corresponding activation volume (V^*) can be calculated from nanoindentation SRJ tests, according to the relationship [53]:

$$V^* = \frac{3\sqrt{3}\,kT}{mH} \quad \text{(VIII)}$$

where k is the Boltzman constant, T the test temperature and H the hardness. Generally, activation volumes are expressed in units of b^3, where b is the Burgers vector [54]. Typically, ~1000 b^3 occurs when dislocations cut through the forest of dislocations and 1–100b^3 for dislocation based plasticity (nucleation and/or cross-slip) [55,56]. For the Cantor alloy, an activation volume of 62b^3 is obtained and therefore dislocation-dislocation interactions are deemed responsible for the plastic deformation. This value is similar to that observed in BCC metals (8–100b^3) and HCP metals (5–100b^3), yet smaller than that seen for CG FCC metals (10^2~10^3 b^3) [57]. The relatively low value of V^* suggests that dislocations glide over the obstacles with high friction stress. The value for V^* is much smaller than in conventional FCC metals, which can be attributed to the presence of heterogeneities in the HEA that make the dislocation movement intermittent ("nanoscale segment detrapping") [23,58]. The pronounced change in hardness after a strain rate change and thus the high values of the SRS for the FCC CoCrFeMnNi HEA could be attributed to the significant solid solution hardening contribution, which needs to be thermally overcome [28].

3.6. Transmission electron microscopy

To better understand the evolution of the microstructure of the CoCrFeMnNi HEA during SP deformation, TEM analysis was performed on the material both in the as-cast condition (Fig. 11) and after SP testing under a displacement rate of 2 mm·min^{-1} (Fig. 12). The analysis was performed at this displacement rate since it is the one for which the most work-hardening was observed and therefore, the most significant microstructural differences would be anticipated. In the as-cast condition, some nanograins were detected. Therefore the microstructure consists of bimodal grains, showing micrometer-sized grains (Fig. 1a and b) and ultrafine (20–70 nm) grains (Fig. 11). These grains would correspond to the FCC crystalline phase as deduced from XRD (Fig. 1c).

As shown in Fig. 5a, among all the displacement rates used during SP testing, the highest F_{MAX} value was achieved when testing at 2 mm·min^{-1} due to the work-hardening process. Upon inspection of the fractured test specimen, TEM samples were extracted from the zone of maximum stress, located on the lower surface of the specimen opposite to where the punch contacts the specimen (see red colour in Fig. 8), where the stress reaches approximately 5.5 × 10^8 Pa. The size of the grains are smaller than 50 nm and therefore grain refinement has taken place. The considerable amount of plastic deformation observed when SP testing under a displacement rate of 2 mm·min^{-1}, and the resultant grain refinement that takes place even at room temperature, is consistent with observations of grain refinement in high pressure torsion of CoCrFeMnNi HEA materials at room temperature [59]. The grain refinement is attributed to the multiple twin-twin interactions (Fig. 12a), which can result in severe lattice distortion and the formation of multiple dislocations at these interaction areas. It has previously been reported that significant plastic deformation can result in grain refinement by combined dislocation activities and deformation twinning [60]. Grain refinement has been widely observed in FCC materials with low stacking fault energies (SFE) [60], including CoCrFeMnNi HEA [61], but has yet to be reported in CoCrFeMnNi HEA material subjected to SP testing at room temperature, at the relatively slow rate of displacement of 2 mm·min^{-1}.

For ultrafine grained Cu with nano-twins, a high value of the work-hardening exponent n is detected (~ 0.66) [62] due to the strong interaction between dislocations and nanotwins. On the other hand, in the case of ultrafine grained FCC Cu with nano-twins, the value of n is 0.66 and the twin thickness is 4 nm [62]. The reason for the high n value is the presence of nano-twins, the dislocation-nanotwin interaction and the large intragranular dislocation storage at twin boundary interfaces. In the current study, slightly smaller n

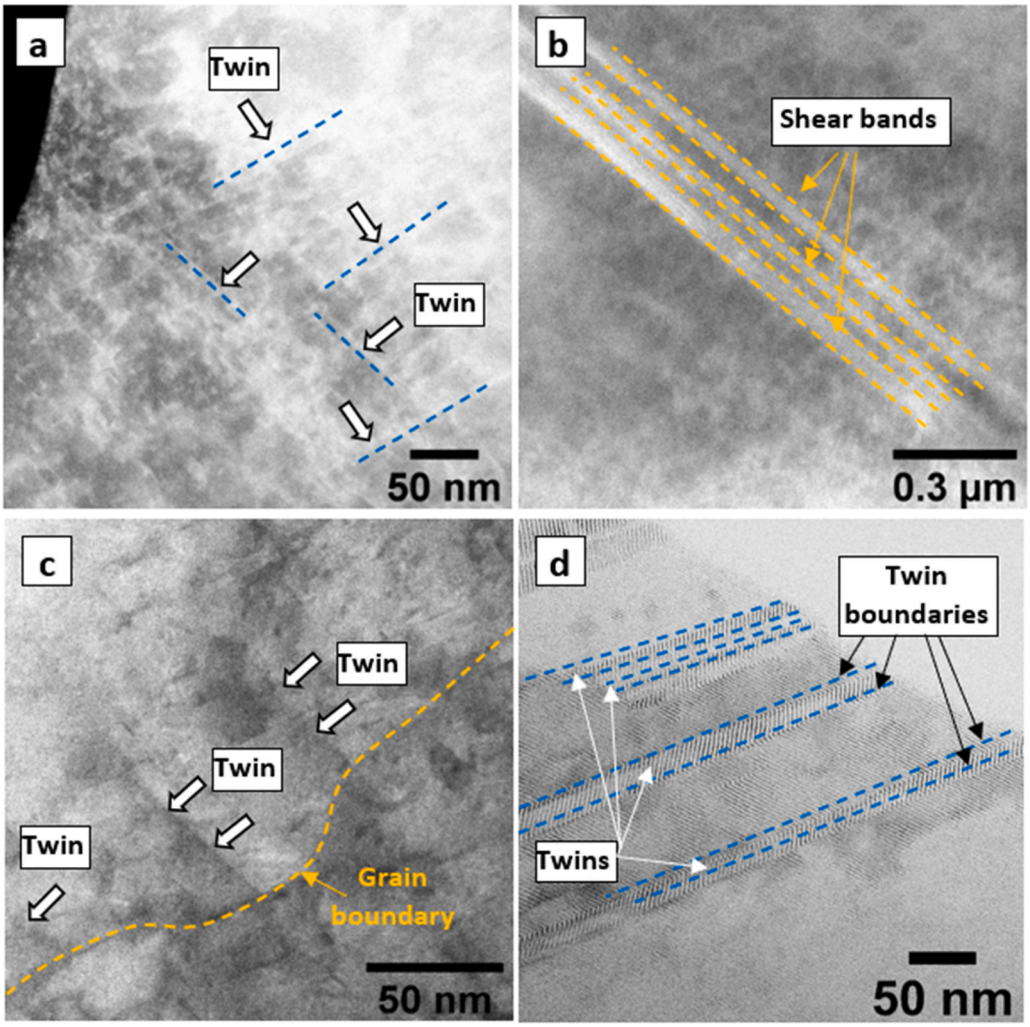

Fig. 12. TEM images for CoCrFeMnNi HEA punch tested at 2 mm·min^{-1} until failure showing a) and c) twins, d) twins and twin boundaries and c) shear bands.

values have been obtained (Table 1), from 0.34 to 0.5, thus indicating the increased ductility of the material by delaying the onset of neck formation. Twinning deformation was also observed in other HEAs at various deformation conditions [39], which is the main reason for the observed large work hardenability. The low activation volume of dislocations in HEAs is attributed to the high density of intrinsic obstacles, which can also lead to increased dislocation storage due to the higher dislocation-dislocation intersection which therefore result in large work hardenability. The extensive work hardening in FCC HEAs is mainly due to deformation twinning and the subsequent interaction of dislocations with the deformation twins. Zaddach et al. [63] observed that the SFE decreased with the increase in the number of elements in the equi-atomic entropy alloys and the SFE values for the quinary HEAs are in the twinning induced plasticity regime.

From the TEM images of the SP tested sample (Fig. 12a), twins of approximately 0.3 μm thickness and 50 nm length, which cross each other and propagate at 45°, can be observed. The abundant presence of these short twins indicate that they arrest before they can propagate, thus indicating the large interactions with twins and grain boundaries (Fig. 12c) that tend to arrest them. These twins are similar to those reported by other authors for CoCrFeMnNi HEA [64] when subjected to tensile loading at − 196 °C, where work-hardening is expected to be most significant. This suggests that SP testing, where the material is subjected to a biaxial stress state, promotes twinning and therefore plastic deformation, more than that typically observed under tensile deformation. Deformation twinning is also promoted by a low SFE, low temperature and high strain rate [65]. Generally, in low-SFE materials, such as CoCrFeMnNi HEA (~20–25 mJ m^{-2}) [63], dislocation cross-slip and climb is impeded, as dissociation into partial dislocations with a wide spacing is more energetically favourable and therefore they are more likely to deform by twinning.

Multiple shear bands are observed rather than a single shear band, therefore localised shear is prevented. This can also contribute towards the excellent strain-hardening and low thermal softening taking place. No adiabatic shear localisation is observed, therefore the strain rate deformation is not significant enough to result in a temperature rise in the narrow region of a single shear band [66]. The twinning-induced continuous strain-hardening observed suppresses shear localisation in competition with the thermal softening effect. A critical shear strain for shear localisation was proposed by Staker [67], according to the relationship:

$$\gamma_c = \frac{\rho C_p n}{-\frac{\partial \tau}{\partial T}} \tag{IX}$$

where $\rho = 7.9\ \mathrm{kg/m^3}$ is the density, C_p is the specific heat capacity ~450 J/(kgK) for Cantor alloy [51] and parameter n is the strain hardening power index. The term $\rho C_p n$ is the hardening component while $\frac{d\tau}{dT}$ is the competing thermal softening parameter. The value of $\rho C_p n$ for CrMnFeCoNi HEA is approximately 630 kPa/K, which equates to around 70% of that of Cu [58], which is consistent with the

excellent work hardening capability even under SP loading (Fig. 5), and the high resistance to shear localisation.

4. Conclusions

The research presented in this paper has examined the suitability of determining the strain rate sensitivity (SRS) of the high-entropy alloy (HEA) alloy CoCrFeMnNi by small punch (SP) testing. From this work, the following conclusions can be drawn:

- A CoCrFeMnNi HEA produced directly upon suction casting (cooling rate ~250 K/s) without subsequent homogenisation results in a bimodal microstructure of micrometer-sized and ultrafine (20–70 nm) grains containing heterogeneities. These include Co-Cr-Fe-enriched and Mn-enriched domains with Ni constant throughout both regions. The relative high ductility and strength, despite the presence of casting defects, could be attributed to the presence of these heterogeneities and to the bimodal microstructure.

- SP testing has been proven to be an efficient method of calculating the SRS of CoCrFeMnNi HEA for displacement rates ranging from 0.2 to 2 mm·min^{-1} at room temperature despite the presence of casting defects induced upon suction casting. This could be of industrial interest for low-cost assessment of the SRS of expensive materials by using a small specimen size.
- The maximum displacement rate for SP testing is limited by the presence of casting defects induced during the suction casting process. However, suitable results were obtained for displacement rates ranging from 0.2 to 2 mm·min^{-1}.
- Finite element analysis (FEA) simulations indicate that the von Mises stresses and the plastic strains are initially concentrated in the regions directly opposite to where the specimen is in contact with the punch head and at the clamped regions between the disc and die set. The stress was found to increase as the displacement rate was raised from 0.2 to 2 mm·min^{-1}, whereas the plastic strain distributions are similar in all cases.
- The SRS obtained from SP experiments was found to be m = 0.1387 while the FEA simulations predicted a slightly smaller value, of m = 0.1313. This latter value is closer to that obtained if the material was completely free from casting defects, as indicated by nanoindentation jump tests, which was capable of characterising the mechanical behaviour whilst being insensitive to the presence of small casting defects.
- For the CoCrFeMnNi HEA alloy, an activation volume of 62b^3 was obtained, providing guidance that dislocation-dislocation interactions are primarily responsible for the nature of plastic deformation.
- The relationship between the experimental and the empirically derived predicted properties from the SP tests revealed a high level of agreement for maximum stress properties. The properties predicted at 2 mm·min^{-1} (R^2 = 0.96) offered a stronger fit than at 0.5 mm·min^{-1} (R^2 = 0.92).

CRediT authorship contribution statement

S. González: Conceptualization, Writing – original draft, Writing – review & editing, Analysis. **A. K. Sfikas:** Data curation, Visualization, Investigation. **Spyros Kamnis:** Funding acquisition, Investigation. **S.E. John:** Data curation, Investigation. **Z.W. Nye:** Data curation, Investigation. **M. Spink:** Data curation, Visualization, Analysis. **C. Allen:** Data curation, Visualization. **R. Martínez-Sánchez:** Writing – review & editing. **S.W. Naung:** Data curation, Investigation, Writing – review & editing. **M. Rahmati:** Investigation, Analysis, Supervision. **T. Keil:** Data curation, Investigation, Writing – review & editing. **K. Durst:** Analysis, Investigation. **R.J. Lancaster:** Analysis, Investigation, Writing – review & editing.

Data availability

Data will be made available on request.

Declaration of Competing Interest

The authors declare the following financial interests/personal relationships which may be considered as potential competing interests: Spyros Kamnis reports financial support was provided by UK Research and Innovation. Sergio Gonzalez Sanchez reports equipment, drugs, or supplies and travel were provided by Diamond Light Source Ltd. K. Dust reports equipment, drugs, or supplies was provided by German Research Foundation (DFG). Spyros Kamnis reports a relationship with Castolin Eutectic Ltd that includes: employment. NA has patent NA pending to NA. NA.

Acknowledgements

The authors would like to acknowledge the support from the UK Research & Innovation (UKRI-IUK) national funding agency. Project Grant: 53662 'Design of High-Entropy Superalloys Using a Hybrid Experimental-Based Machine Learning Approach: Steel Sector Application'. The authors would also like to thank Diamond Light Source for access and support in use of the electron Physical Science Imaging Centre (Instrument E01 or/and E02 and proposal number MG28409) that contributed to the results presented here. K.D. gratefully acknowledge the funding by the German Research Foundation (DFG) within the priority programme SPP2006 under Grant No. DU424/13–2.

References

[1] A. Poulia, E. Georgatis, C. Mathiou, A.E. Karantzalis, Phase segregation discussion in a $Hf_{25}Zr_{30}Ti_{20}Nb_{15}V_{10}$ high entropy alloy: The effect of the high melting point elements, Mater. Chem. Phys. 210 (2018) 251–258.
[2] S.P. O'Brien, J. Christudasjustus, L. Esteves, S. Vijayan, J.R. Jinschek, N. Birbilis, R.K. Gupta, A low-cost, low-density, and corrosion resistant AlFeMnNi compositionally complex alloy, npj Mater. Degrad. 5 (2021) 12.
[3] A. Poulia, E. Georgatis, A. Lekatou, A.E. Karantzalis, Microstructure and wear behavior of a refractory high entropy alloy, Int. J. Refr. Met. Hard Mater. 57 (2016) 50–63.
[4] J.W. Yeh, Recent progress in high-entropy alloys, Ann. De. Chim. - Sci. De. Mater. 31 (2006) 633–648.
[5] J.W. Yeh, S.K. Chen, S.J. Lin, J.Y. Gan, T.S. Chin, T.T. Shun, C.H. Tsau, S.Y. Chang, Nanostructured high-entropy alloys with multiple principal elements: novel alloy design concepts and outcomes, Adv. Eng. Mater. 6 (2004) 299–303.
[6] B. Cantor, I.T.H. Chang, P. Knight, A.J.B. Vincent, Microstructural development in equiatomic multicomponent alloys, Mater. Sci. Eng. A 375–377 (2004) 213–218.
[7] B. Gludovatz, A. Hohenwarter, D. Catoor, E.H. Chang, E.P. George, R.O. Ritchie, A facture-resistant high-entropy alloy for cryogenic applications, Science 345 (2014) 1153–1158.
[8] J. Torres, A.P. Gordon, Mechanics of the small punch test: a review and qualification of additive manufacturing materials, J. Mater. Sci. 56 (2021) 10707–10744.
[9] R.J. Lancaster, H.W. Illsley, G.R. Davies, S.P. Jeffs, G.J. Baxter, Modelling the small punch tensile behaviour of an aerospace alloy, Mater. Sci. Technol. 33 (9) (2017) 1065–1073.
[10] R.J. Lancaster, S.P. Jeffs, B.J. Haigh, N.C. Barnard, Derivation of material properties using small punch and shear punch test methods, Mater. Des. 215 (2022) 110473.
[11] S. Davies, S. Jeffs, R. Lancaster, G. Baxter, High temperature deformation mechanisms in a DLD nickel superalloy, Materials 10 (2017) 457.
[12] R.C. Hurst, R.J. Lancaster, S.P. Jeffs, M.R. Bache, The contribution of small punch testing towards the development of materials for aero-engine applications, Theor. Appl. Fract. Mech. 86, Part A (2016) 69–77.
[13] J.M. Park, J. Moon, J.W. Bae, M.J. Jang, J. Park, S. Lee, H.S. Kim, Strain rate effects of dynamic compressive deformation on mechanical properties and microstructure of CoCrFeMnNi high-entropy alloy, Mater. Sci. Eng.: A 719 (2018) 155–163.
[14] A. Huang, S. Fensin, M.A. Meyers, Strain-Rate Effects and Dynamic Behavior of High Entropy Alloys, J. Mater. Res. Technol. (2022), https://doi.org/10.1016/j.jmrt.2022.11.057
[15] A. Raturi, K. Biswas, N.P. Gurao, A mechanistic perspective on the kinetics of plastic deformation in FCC High Entropy Alloys: Effect of strain, strain rate and temperature, Scr. Mater. 197 (2021) 113809.

[16] M.A. Meyers, Dynamic Behavior of Materials, JohnWiley and Sons, New York, 1994.
[17] R.J. Asaro, S. Suresh, Mechanistic models for the activation volume and rate sensitivity in metals with nanocrystalline grains and nano-scale twins, Acta Mater. 53 (2005) 3369–3382.
[18] M. Shabanisamghabady, Effect of strain rate on the tensile behaviour of CoCrFeNi and CoCrFeMnNi High Entropy Alloys (Thesis), Clempson university, 2018.
[19] Q. Wei, Strain rate effects in the ultrafine grain and nanocrystalline regimes—influence on some constitutive responses, J. Mater. Sci. 42 (2007) 1709–1727.
[20] F. Lowrie, M. Gorley, E. Surrey, B. Wynne, D. Wilkes, Strain Rate Sensitivity Effect Measured in 316 Steel by the Small Punch Testing Method, Mater. Perform. Charact. 7 (2018) 376–383.
[21] R.B. Figueiredo, W. Wolf, T.G. Langdon, Effect of grain size on strength and strain rate sensitivity in the CrMnFeCoNi high-entropy alloy, J. Mater. Res. Technol. 20 (2022) 2358–2368.
[22] Y. Zhao, X. Wang, T. Cao, J.-K. Han, M. Kawasaki, J.-il Jang, H.N. Han, U. Ramamurty, L. Wang, Y. Xue, Effect of grain size on the strain rate sensitivity of CoCrFeNi high-entropy alloy, Mat. Sci. Eng.: A 782 (2020) 139281.
[23] E. Ma, X. Wu, Tailoring heterogeneities in high-entropy alloys to promote strength–ductility synergy, Nat. Commun. 10 (2019) 5623.
[24] E. Ma, T. Zhu, Towards strength–ductility synergy through the design of heterogeneous nanostructures in metals, Mater. Today 20 (2017) 323–331.
[25] BS EN 10371:2021 Metallic materials - Small punch test method (2021) 1–60.
[26] ASTM 61832 Standard Test Method for Small Punch Testing of Metallic Materials, " (2020) 1–12.
[27] S. Davies, S. Jeffs, R. Lancaster, G. Baxter, High temperature deformation mechanisms in a DLD nickel superalloy, Materials 10 (2017) 457.
[28] Verena Maier-Kiener, Benjamin Schuh, Easo P. George, Helmut Clemens, Anton Hohenwarter, Nanoindentation testing as a powerful screening tool for assessing phase stability of nanocrystalline high-entropy alloys, Mater. Des. 115 (2017) 479–485.
[29] Tom Keil, Shabnam Taheriniya, Enrico Bruder, Gerhard Wilde, Karsten Durst, Effects of solutes on thermal stability, microstructure and mechanical properties in CrMnFeCoNi based alloys after high pressure torsion, Acta Mater. 227 (2022) 117689.
[30] X. Lin, W. Johnson, J. Appl. Phys. 78 (1995) 6514.
[31] George F. Vander Voort. ASM Handbook: Metallography and Microstructures, American Society for Metals, Metals Park, 9, 2004.
[32] Z. Li, S. Zhao, S.M. Alotaibi, Y. Liu, B. Wang, M.A. Meyers, Adiabatic shear localization in the CrMnFeCoNi high-entropy alloy, Acta Mater. 151 (2018) 424–431.
[33] B.E. MacDonald, Z. Fu, X. Wang, Z. Li, W. Chen, Y. Zhou, D. Raabe, J. Schoenung, H. Hahn, E.J. Lavernia, Influence of phase decomposition on mechanical behavior of an equiatomic CoCuFeMnNi high entropy alloy, Acta Mater. 181 (2019) 25–35.
[34] Brad L. Boyce, Thomas B. Crenshaw, and Morris F. Dilmore. The Strain-Rate Sensitivity of High- Strength High-Toughness Steels. Sandia National Laboratories Albuquerque, New Mexico (2007).
[35] R.W. Hertzberg, Deformation and fracture mechanics of Engineering Materials, 4th edition.,, John Wiley & Sons, Inc., Hoboken, 1996.
[36] F. Khodabakhshi, M. Haghshenas, H. Eskandari, B. Koohbor, Hardness–strength relationships in fine and ultra-fine grained metals processed through constrained groove pressing, Mater. Sci. Eng.: A 636 (2015) 331–339.
[37] Bruchhausen, S. Holmström, I. Simonovski, T. Austin, J.-M. Lapetite, S. Ripplinger, F. de Haan, Recent developments in small punch testing: Tensile properties and DBTT, Theor. Appl. Fract. Mech. 86 (Part A) (2016) 2–10.
[38] A.B. Geltmacher. PhD thesis: A modelling study of the effect of stress state on void linking during ductile fracture. The Pennsylvania State University ProQuest Dissertations Publishing (1994) 9428102.
[39] M. Komarasamy, K. Alagarsamy, R.S. Mishra, Serration behavior and negative strain rate sensitivity of Al0.1CoCrFeNi high entropy alloy, Intermetallics 84 (2017) 20–24.
[40] C. Rodríguez, J. García, E. Cárdenas, C. Betegón, Mechanical properties characterization of heat-affected zone using the small punch test, Weld. J. 88 (2009) 188–192.
[41] T.E. García, C. Rodríguez, F.J. Belzunce, C. Suárez, Estimation of the mechanical properties of metallic materials by means of the small punch test, J. Alloy. Compd. 582 (2014) 708–717.
[42] L. Xue, X. Ling, S. Yang, Mechanical behaviour and strain rate sensitivity analysis of TA2 by the small punch test, Theor. Appl. Fract. Mech. 99 (2019) 9–17.
[43] F. Wang, B. Li, T.T. Gao, P. Huang, K.W. Xu, T.J. Lu, Activation volume and strain rate sensitivity in plastic deformation of nanocrystalline Ti, Surf. Coat. Technol. 228 (2013) S254–S256.
[44] R.P. Carreker Jr., W.R. Hibbard Jr., Tensile deformation of high-purity copper as a function of temperature, strain rate and grain size, Acta Metal. 1 (1953) 654–663.
[45] P.S. Follansbee, G. Regazzoni, U.F. Kocks, Transition to drag-controlled deformation in copper at high strain rates, Inst. Phys. Conf. 70 (1984) 71–80.
[46] Q. Wei, S. Cheng, K.T. Ramesh, E. Ma, Effect of nanocrystalline and ultrafine grain sizes on the strain rate sensitivity and activation volume: fcc versus bcc metals, Mater. Sci. Eng.: A 381 (2004) 71–79.
[47] W. Nix, H. Gao, Indentation Size Effects In Crystalline Materials: A Law For Strain Gradient Plasticity, J. Mech. Phys. Solids 46 (1998) 411–425.
[48] B. Gludovatz, E.P. George, R.O. Ritchie, Processing, Microstructure and Mechanical Properties of the CrMnFeCoNi High-Entropy Alloy, JOM 67 (2015) 2262–2270.
[49] Y.Z. Wang, Z.M. Jiao, G.B. Bian, H.J. Yang, H.W. He, Z.H. Wang, P.K. Liaw, J.W. Qiao, Dynamic tension and constitutive model in $Fe_{40}Mn_{20}Cr_{20}Ni_{20}$ high-entropy alloys with a heterogeneous structure, Mater. Sci. Eng.: A 839 (2022) 14283.
[50] K. Wang, X. Jin, Y. Zhang, P.K. Liaw, J. Qiao. Phys. Rev. Mat. 5 (2021) 113608.
[51] T. Keil, E. Bruder, M. Laurent-Brocq, K. Durst, From diluted solid solutions to high entropy alloys: Saturation grain size and mechanical properties after high pressure torsion, Scr. Mater. 192 (2021) 43–48.
[52] M.A. Monclús, J.M. Molina-Aldareguia, in: Handbook of Mechanics of Materials, (2018) 1–29.
[53] V. Maier, K. Durst, J. Mueller, B. Backes, H.W. Höppel, M. Göken, Nanoindentation strain-rate jump tests for determining the local strain-rate sensitivity in nanocrytalline Ni and ultrafine-grained Al, J. Mater. Res. 26 (2011) 1421–1430.
[54] M.A. Meyers, A. Mishra, D.J. Benson, Mechanical properties of nanocrystalline materials, Prog. Mater. Sci. 51 (2006) 427–556.
[55] Y. Xiao, Y. Zou, A.S. Sologubenko, R. Spolenak, J.M. Wheeler, Size-dependent strengthening in multi-principal element, face-centered cubic alloys, Mater. Des. 193 (2020) 108786.
[56] Xu-Sheng Yang, Yun-Jiang Wang, Guo-Yong Wang, Hui-Ru Zhai, L.H. Dai, Tong-Yi Zhang, Time, Stress and temperature-dependent deformation in nanostructured copper: Stress relaxation tests and simulations, Acta Mater. 108 (2016) 252–263.
[57] S.I. Hong, J. Moon, S.K. Hong, H.S. Kim, Thermally activated deformation and the rate controlling mechanism in CoCrFeMnNi high entropy alloy, Mater. Sci. Eng: A 682 (2017) 569–576.
[58] Q.-J. Li, H.W. Sheng, E. Ma, Strengthening in multi-principal element alloys with local-chemical-order roughened dislocation pathways, Nat. Commun. 10 (2019) 3563.
[59] W. Wu, M. Song, S. Ni, J. Wang, Dual mechanisms of grain refinement in a FeCoCrNi high-entropy alloy processed by high-pressure torsion, Sci. Rep. 7 (2017) 46720.
[60] Y.B. Wang, X.Z. Liao, Y.H. Zhao, E.J. Lavernia, S.P. Ringer, Z. Horita, T.G. Langdon, Y.T. Zhu, The role of stacking faults and twin boundaries in grain refinement of a Cu–Zn alloy processed by high-pressure torsion, Mater. Sci. Eng. A 527 (2010) 4959–4966.
[61] N. Stepanov, M. Tikhonovsky, N. Yurchenko, D. Zyabkin, M. Klimova, S. Zherebtsov, A. Efimov, G. Salishchev, Effect of cryo-deformation on structure and properties of CoCrFeNiMn high-entropy alloy, Intermetallics 59 (2015) 8–17.
[62] L. Lu, Z.S. You, K. Lu, Work hardening of polycrystalline Cu with nanoscale twins, Scr. Mater. 66 (2012) 837–842.
[63] A. Zaddach, C. Niu, C. Koch, D. Irving, Mechanical properties and stacking fault energies of NiFeCrCoMn high-entropy alloy, JOM 65 (2013) 1780–1789.
[64] J. Xie, H. Dong, Y. Hao, Z. Fan, C.-A. Wang, Exploring the formation mechanism of deformation twins in CrMnFeCoNi High Entropy Alloy, Acta Metall. Sin. 35 (2022) 1275–1280.
[65] Y. Zhu, X. Liao, X. Wu, Deformation twinning in nanocrystalline materials, Prog. Mater. Sci. 57 (2012) 1–62.
[66] M.A. Meyers, Z. Li, S. Zhao, B. Wang, Y. Liu, P.K. Liaw, Shear localization of fcc high-entropy alloys, E. P. J. Web Conf. 183 (2018) 03028.
[67] M.R. Staker, The relation between adiabatic shear instability strain and materials properties, Acta Met. 29 (1981) 683–689.